Journal of Computational Physics **165,** 334–353 (2000)
doi:10.1006/jcph.2000.6611, available online at http://www.idealibrary.com on IDEAL®

A High-Order Finite-Difference Algorithm for the Analysis of Standing Acoustic Waves of Finite but Moderate Amplitude

Christian Vanhille* and Cleofé Campos-Pozuelo†

**Área de Matemática Aplicada, Escuela Superior de Ciencias Experimentales y Tecnología, Universidad Rey Juan Carlos, C. Tulipán s/n, 28933 Móstoles, Madrid, Spain; and †Instituto de Acústica, Consejo Superior de Investigaciones Científicas, C. Serrano 144, 28006 Madrid, Spain*
E-mail: c.vanhille@escet.urjc.es, ccampos@ia.cetef.csic.es

Received November 29, 1999; revised August 23, 2000

A numerical formulation for modelling standing acoustic waves of finite but moderate amplitude is presented. A thermoviscous fluid contained in a one-dimensional tube with rigid walls is considered. The fluid is initially at rest and is excited by means of a harmonic piston. A second-order wave equation for viscous and homogeneous fluids is used. The perturbation method is employed. The numerical simulation is carried out by a multi-time-step, implicit, six-point finite-difference scheme of high order in the time domain. Displacement and pressure waveforms and distributions are presented. Numerical results are validated by comparison with an analytical model. The numerical scheme is illustrated with several examples.

Key Words: numerical simulation; finite-difference scheme; nonlinear acoustics; standing waves; time-domain analysis.

1. INTRODUCTION

High-intensity ultrasonic waves are becoming increasingly useful in industrial processing for applications such as particle agglomeration, liquid atomization, cleaning, control of foam, and drying. These applications are possible because of the nonlinear effects produced by high-frequency and finite-amplitude pressures—macrosonic waves. The efficiency of this industrial processing is based on the intense nonlinear acoustic field established within the treatment chamber. Therefore, knowledge of the distribution of the nonlinear pressure inside bounded cavities is important for developing practical systems. When amplitudes are infinitesimal, the acoustic waves can be described by linear laws. When the acoustic-pressure amplitude becomes finite, the equations of motion are nonlinear. We present a new numerical procedure for the study of standing acoustic waves of finite but moderate amplitude.

0021-9991/00 $35.00

Several papers have presented analytical studies of the propagation of nonlinear waves [1, 2], as well as the behaviour of nonlinear standing waves [3, 4]. The physical basis of nonlinear acoustics has also been reviewed [5–9].

Numerical methods applied to the study, modelling, and design of complex sonic or ultrasonic systems are usually based on the finite-element method or the boundary-element method, or the coupling of both methods [10–12]. They use the well-known Helmholtz equation to describe the linear acoustical behaviour of infinitesimal amplitude waves.

On the other hand, various numerical methods have been developed for studying progressive nonlinear waves [13–16]. They are generally based on the finite-difference method. A very good review is also available (see Section 11 of Ref. [9]). Far fewer numerical developments exist for standing waves. Of special interest is the recent paper by Ilinskii *et al.* [17], which presents an algorithm in the frequency domain based on the Runge–Kutta method. The model in Ref. [17] is valid for one-dimensional nonlinear standing waves in an ideal gas. Their mathematical model considers a one-dimensional resonator of arbitrary shape.

We propose a numerical algorithm for the study of standing acoustic waves of finite but moderate amplitude. Based upon the finite-difference method, it operates in the time domain [18]. A second-order wave equation written in Lagrangian coordinates is considered [5]. Losses due to dissipation of the fluid are taken into account, but losses due to the walls of the tube are not considered. Dissipation losses are represented by a third-order partial derivative of the displacement. The dissipation values are not limited [19].

This work constitutes the first step of a more ambitious and general project. The final objective is to have a useful tool for designing systems for high-power ultrasonic applications (e.g., sonochemical reactors, systems for acoustic agglomeration, and compressors) that includes nonlinear effects. This means that strongly nonlinear waves, three-dimensional cavities, etc., will have to be modelled. The moderate-amplitude case treated here is the first step. The validation of its numerical approximation will provide a solid foundation for constructing successive future models.

2. FUNDAMENTAL EQUATIONS

The paper by Beyer [5] is one of the most complete reviews of the state of the art in nonlinear acoustics. It includes the basic equations of nonlinear acoustics, as well as the most important contributions to the development of the field throughout its history.

We consider finite-amplitude standing waves in a homogeneous and thermoviscous fluid. Only the terms up to the second order in the acoustic Mach number defined by $p_{ac}/\rho_0 c_0^2$ are considered, where p_{ac} is the acoustic pressure, ρ_0 the density of the medium at rest, and c_0 the small-signal sound speed.

As is well known, a mechanical system can be described using two kinds of coordinate systems: Lagrangian (or material) coordinates and Eulerian (or spatial) coordinates [19]. The systems are equivalent when infinitesimal-amplitude perturbations are studied but have important differences when finite-amplitude perturbations are analysed. We use Lagrangian coordinates.

To obtain the second-order one-dimensional wave equation, the state equation for an isentropic fluid [9, Chap. 2] and the conservation of the mass and momentum are considered.

These equations, without external forces, can be written for a viscous fluid as

$$p = P\left(\frac{\rho}{\rho_0}\right)^{\gamma} - Q \tag{1}$$

$$\frac{\rho_0 - \rho}{\rho} = \frac{\partial u}{\partial x} \tag{2}$$

$$\rho_0 \frac{\partial^2 u}{\partial t^2} = -\frac{\partial p}{\partial x} + \rho_0 \nu b \frac{\partial^3 u}{\partial t \partial x^2}, \tag{3}$$

where p is the pressure, ρ is the density of the fluid, u is the displacement of the particle, γ is the relation of specific heats, $P = \rho_0 c_0^2/\gamma$, and νb is a parameter which gives an idea of the viscosity of the medium—ν is the kinematic viscosity and $b = \frac{4}{3} + \frac{\eta'}{\eta}$, η' and η being the viscosities of the medium [5]. Q is a characteristic parameter of the fluid. For an ideal gas, $Q = 0$, and for sea water $Q = 3$ kbar [20]. More details about the applicability of the state equation (1) can be found in Ref. [20]. From Eqs. (1) and (2) it is easy to obtain

$$\frac{\partial p}{\partial x} = -P\gamma \left(1 \Big/ \left(1 + \frac{\partial u}{\partial x}\right)^{\gamma+1}\right) \frac{\partial^2 u}{\partial x^2}. \tag{4}$$

Equation (4) can be approximated by an expansion in Taylor series in terms of the small parameter $\frac{\partial u}{\partial x}$ (of the order of the acoustic Mach number) up to the second order:

$$\frac{\partial p}{\partial x} = -P\gamma \frac{\partial^2 u}{\partial x^2}\left[1 - (\gamma+1)\frac{\partial u}{\partial x}\right]. \tag{5}$$

Combining Eqs. (5) and (3), we obtain the following second-order wave equation in Lagrangian coordinates:

$$\rho_0 \frac{\partial^2 u}{\partial t^2} = P\gamma \frac{\partial^2 u}{\partial x^2} - P\gamma \frac{(\gamma+1)}{2} \frac{\partial}{\partial x}\left[\left(\frac{\partial u}{\partial x}\right)^2\right] + \rho_0 \nu b \frac{\partial^3 u}{\partial t \partial x^2}. \tag{6}$$

The value of γ determines the nonlinear behaviour of the fluid and can be found in the literature for the most common fluids (see for instance the chapter by Beyer in Ref. 9). Very often this equation is written in terms of the so-called nonlinearity parameter β, defined as $\beta = \frac{\gamma+1}{2}$.

To solve the second-order wave equation (6) the perturbation method is applied. The solution for the displacement of the particle is assumed to be the addition of two terms, the linear solution u_1 plus a second-order correction u_2,

$$u = u_1 + u_2. \tag{7}$$

u_2 must be much smaller than u_1 ($u_2 \ll u_1$). Since u_1 represents the linear solution, it has to verify

$$\rho_0 \frac{\partial^2 u_1}{\partial t^2} = P\gamma \frac{\partial^2 u_1}{\partial x^2} + \rho_0 \nu b \frac{\partial^3 u_1}{\partial t \partial x^2}. \tag{8}$$

Truncating all the terms of third or higher order, the equation for the perturbation term u_2 is

$$\rho_0 \frac{\partial^2 u_2}{\partial t^2} = P\gamma \frac{\partial^2 u_2}{\partial x^2} + \rho_0 \nu b \frac{\partial^3 u_2}{\partial t \partial x^2} - P\gamma \frac{(\gamma+1)}{2} \frac{\partial}{\partial x}\left[\left(\frac{\partial u_1}{\partial x}\right)^2\right]. \tag{9}$$

If the system has a harmonic excitation, u_1 will have a unique spectral component centred at the excitation frequency, while u_2 will present the double and zero frequencies.

In line with our second-order approximation, the state equation (1) can be written as an expansion in Taylor series in terms of the parameter $(\rho_0 - \rho)/\rho_0$ (of the same order as the acoustic Mach number). The resulting equation is combined with Eq. (2), to which the same approximation has been applied. In this way the following expressions for the linear pressure p_1 and the second-order perturbation p_2 are obtained

$$p_1 = -P\gamma \frac{\partial u_1}{\partial x} - Q, \qquad p_2 = -P\gamma \frac{\partial u_2}{\partial x} + \frac{P\gamma}{2}(\gamma+1)\left(\frac{\partial u_1}{\partial x}\right)^2. \tag{10}$$

The fluid is at complete rest at its initial state, $t = 0$, and is then excited by harmonic motion of a piston at $x = 0$ at the pulsation ω ($\omega = 2\pi f$ where f is the frequency). The following initial and boundary conditions are added to Eqs. (8) and (9), L being the length of the tube:

for the linear displacement,

$$\begin{aligned} &x = 0 \qquad && u_1(0,t) = u_0 \sin(\omega t) \\ &x = L \qquad && u_1(L,t) = 0 \\ &t = 0 \qquad && \begin{cases} u_1(x,0) = 0 \\ \frac{\partial u_1(x,0)}{\partial t} = 0 \qquad (\forall x \neq 0), \end{cases} \end{aligned} \tag{11a}$$

for the second-order component of the displacement,

$$\begin{aligned} &x = 0 \qquad && u_2(0,t) = 0 \\ &x = L \qquad && u_2(L,t) = 0 \\ &t = 0 \qquad && \begin{cases} u_2(x,0) = 0 \\ \frac{\partial u_2(x,0)}{\partial t} = 0. \end{cases} \end{aligned} \tag{11b}$$

3. FINITE-DIFFERENCE ALGORITHM

In this section, the numerical scheme developed to model nonlinear acoustical phenomena is described. The technique allows the evaluation of the solution u, which is a function of the independent variables x and t. Pressure p is then calculated. Thus, the acoustical behaviour of the fluid in the tube is completely known.

In order to solve the nonlinear acoustical problem described in the preceding Section, a numerical approximation in the time domain has been chosen. Therefore all the frequency components of the second-order correction are taken into account directly by means of only one computation. Bulk viscosity of the fluid appears in the differential equation by

means of a third-order partial derivative. Initially, the fluid is assumed to be absolutely at rest. The transient phase, which occurs just before the steady-state phase (standing wave), is entirely modelled. In this paper, the nonlinearity of the equation is limited to the second order; in the development of the Mach number, all the terms of order 3 or higher are neglected.

3.A. *New Dimensionless Variables*

For numerical purposes it is better to write equations in dimensionless form. With this objective, we create two dimensionless independent variables:

$$X = \frac{x}{L}, \qquad T = \omega t. \tag{12}$$

Therefore spatial and temporal spaces remain dimensionless, but the displacement u and pressure p are still quantities with dimensions. The partial derivatives are then written

$$\begin{gathered} \frac{\partial u}{\partial x} = \frac{1}{L}\frac{\partial u}{\partial X} \qquad \frac{\partial u}{\partial t} = \omega\frac{\partial u}{\partial T} \\ \frac{\partial^2 u}{\partial x^2} = \frac{1}{L^2}\frac{\partial^2 u}{\partial X^2} \qquad \frac{\partial^2 u}{\partial t^2} = \omega^2\frac{\partial^2 u}{\partial T^2} \qquad \frac{\partial^3 u}{\partial x^2 \partial t} = \frac{\omega}{L^2}\frac{\partial^3 u}{\partial X^2 \partial T}. \end{gathered} \tag{13}$$

So, Eqs. (8), (9), and (10) take the forms, respectively,

$$\frac{\partial^2 u_1}{\partial T^2} - \frac{\nu b}{\omega L^2}\frac{\partial^3 u_1}{\partial X^2 \partial T} = \frac{c_0^2}{\omega^2 L^2}\frac{\partial^2 u_1}{\partial X^2} \tag{14a}$$

$$\frac{\partial^2 u_2}{\partial T^2} - \frac{\nu b}{\omega L^2}\frac{\partial^3 u_2}{\partial X^2 \partial T} = \frac{c_0^2}{\omega^2 L^2}\frac{\partial^2 u_2}{\partial X^2} - \frac{c_0^2}{2\omega^2 L^3}(\gamma+1)\frac{\partial}{\partial X}\left[\left(\frac{\partial u_1}{\partial X}\right)^2\right] \tag{14b}$$

$$p_1 = \frac{\rho_0 c_0^2}{L}\frac{\partial u_1}{\partial X} \tag{15}$$

$$p_2 = \frac{\rho_0 c_0^2}{L}\frac{\partial u_2}{\partial x} + \frac{\rho_0 c_0^2}{L^2}\left(1 + \frac{\gamma-1}{2}\right)\left(\frac{\partial u_1}{\partial X}\right)^2. \tag{16}$$

The boundary and initial conditions for Eq. (11) are then written as

$$\begin{aligned} &X = 0 \qquad u_1(0,T) = u_0 \sin(T) \\ &X = 1 \qquad u_1(1,T) = 0 \\ &T = 0 \qquad \begin{cases} u_1(X,0) = 0 \\ \frac{\partial u_1(X,0)}{\partial T} = 0 \qquad (\forall X \neq 0) \end{cases} \end{aligned} \tag{17}$$

$$\begin{aligned} &X = 0 \qquad u_2(0,T) = 0 \\ &X = 1 \qquad u_2(1,T) = 0 \\ &T = 0 \qquad \begin{cases} u_2(X,0) = 0 \\ \frac{\partial u_2(X,0)}{\partial T} = 0. \end{cases} \end{aligned} \tag{18}$$

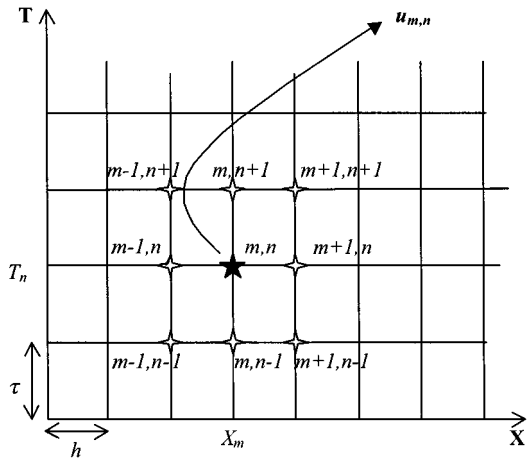

FIG. 1. Discretisation of the dimensionless X–T plane.

3.B. *Mathematical Formulation*

The mathematical formulation employed for the numerical treatment of equations is now presented. The numerical technique is based on the finite-difference method [21, 22].

3.B.1. Discretisation. The discretisation stage begins by subdividing the dimensionless X–T (space–time) plane into sets of equal rectangles of sides $\delta X = h$ and $\delta T = \tau$ with equally spaced grid lines. This process generates a number of NPS points in the dimensionless-spatial space defined by $X_m = (m-1)h$ $(m = 1, \ldots,$ NPS) and a number of NPT points in the dimensionless time space defined by $T_n = (n-1)\tau$ $(n = 1, \ldots,$ NPT), as shown in Fig. 1. Thus, the variable X ranges from 0 to 1 in increments of h; the variable T ranges from 0 to 2π NP in increments of τ, NP being the number of periods desired in the study. We denote by $u_{m,n}$ (respectively $p_{m,n}$) the displacement (respectively pressure) at the node (X_m, T_n) of the plane.

3.B.2. Finite-difference numerical scheme. We now take into account the discretisation in equations. The variable u is now considered to be regular up to the fifth order in $\mathbb{R}^2$ and the variable p up to the second order in $\mathbb{R}^2$. The finite-difference scheme has been developed regarding the bulk-viscosity term: a third-order partial derivative, double in X and single in T. The role of this operator is very important for the formation of the nonlinear standing wave in the tube. For the numerical treatment of this third-order partial derivative $\frac{\partial}{\partial X^2 \partial T}$, an approximation scheme with a high order of truncation error has been developed: a multi-time-step, implicit, six-point scheme. It is allowed by approximation of displacements (functions of two variables) up to the fifth order. By using the "computational molecule" [21], this operator can be expressed as

$$\left.\frac{\partial^3}{\partial X^2 \partial T}\right|_{m,n} = \frac{1}{2h^2\tau} \begin{Bmatrix} (+1)\ldots\ldots & (-2)\ldots\ldots & (+1) \\ \vdots & \vdots & \vdots \\ (0)\ldots\ldots & (0)_{m,n}\ldots\ldots & (0) \\ \vdots & \vdots & \vdots \\ (-1)\ldots\ldots & (+2)\ldots\ldots & (-1) \end{Bmatrix} + O(h^2 + \tau^2). \quad (19)$$

In this way we can represent the other operators of the equations:

$$\left.\frac{\partial^2}{\partial X^2}\right|_{m,n} = \frac{1}{h^2}\{(+1)\ldots\ldots(-2)_{m,n}\ldots\ldots(+1)\} + O(h^2)$$

$$\left.\frac{\partial^2}{\partial T^2}\right|_{m,n} = \frac{1}{\tau^2}\begin{Bmatrix}(+1)\\ \vdots \\ (-2)_{m,n}\\ \vdots \\ (+1)\end{Bmatrix} + O(\tau^2) \tag{20}$$

$$\left.\frac{\partial}{\partial X}\left[\left(\frac{\partial}{\partial X}\right)^2\right]\right|_{m,n} = \frac{1}{h^3}[\{(0)\ldots\ldots(-1)_{m,n}\ldots\ldots(+1)\}^2 - \{(-1)\ldots\ldots(+1)_{m,n}\ldots\ldots(0)\}^2] + O(h) \tag{21}$$

The "computational molecule" used in Eqs. (19), (20) and (21) means that the numbers in the "atoms" (for instance (+1)) are the multipliers of the function values (the displacement u_1 or u_2) at the corresponding mesh points.

From Eqs. (14) the finite-difference approximations for u_1 and u_2 have respectively the order $O(\tau^2) + O(h^2 + \tau^2) + O(h^2)$ and $O(\tau^2) + O(h^2 + \tau^2) + O(h^2) + O(h)$. Therefore both difference equations are respectively consistent with the partial differential equations.

Pressures at grid points are evaluated through a classical progressive finite-difference scheme from the values of the displacement.

Since the numerical scheme is implicit, at each time step, a linear set of (NPS-2) equations with (NPS-2) unknowns has to be solved. The solutions are determined by means of the Gauss method [23].

The computation code is written in FORTRAN 77 and formulated using double precision real numbers. It has been called SNOW-AC (Simulation of NOnlinear Waves in ACoustics).

In the following the stability of the numerical scheme for the equations (8) and (9) is analysed using the von Neumann method [21].

The numerical scheme obtained for u_1 can be written:

$$-\mathrm{A}u_{m-1,n} + (2\mathrm{A}+1)u_{m,n} - \mathrm{A}u_{m+1,n} = -\mathrm{A}u_{m-1,n-2} + (2\mathrm{A}-1)u_{m,n-2} - \mathrm{A}u_{m+1,n-2} + \mathrm{B}u_{m-1,n-1} + 2(1-\mathrm{B})u_{m,n-1} + \mathrm{B}u_{m+1,n-1} \tag{22}$$

with $\mathrm{A} = \nu b\tau/\pi c_0\lambda h^2 = (\nu b/\pi c_0\lambda)(\tau/h^2) = aX$ and $\mathrm{B} = \tau^2/\pi^2 h^2 = (1/\pi^2)(\tau^2/h^2) = bY$; $a > 0, b > 0, X > 0, Y > 0$. We introduce an initial line of errors and we decompose this error at the grid points by a finite Fourier series and we investigate its propagation as t increases. We put $u_{m,n} = e^{i\beta mh}\xi^n$ with the complex number $i = \sqrt{-1}$, β the frequency of the error (which is a real number), and ξ the amplification factor. The substitution of $u_{m,n} = e^{i\beta mh}\xi^n$ into the difference equation (22), after some trigonometric identities and algebraic manipulations, leads to the following algebraic equation:

$$\left(4aX\sin^2\left(\frac{\beta h}{2}\right) + 1\right)\xi^2 + \left(4bY\sin^2\left(\frac{\beta h}{2}\right) - 2\right)\xi + \left(1 - 4aX\sin^2\left(\frac{\beta h}{2}\right)\right) = 0. \tag{23}$$

The roots of Eq. (23) are

$$\xi_1 = \frac{B}{2A} + \frac{\sqrt{B^2 - 4A(-A+2)}}{2A}$$
$$\xi_2 = \frac{B}{2A} - \frac{\sqrt{B^2 - 4A(-A+2)}}{2A}, \tag{24}$$

where $A = 4aX\sin^2(\frac{\beta h}{2}) + 1$ and $B = 2 - 4bY\sin^2(\frac{\beta h}{2})$. If $|\xi| \leq 1$ the numerical scheme is stable [21, 24]. It can be seen that $4aX\sin^2(\frac{\beta h}{2}) \geq 0$ and $2bY\sin^2(\frac{\beta h}{2})/(4aX\sin^2(\frac{\beta h}{2}) + 1) \geq 0$ and therefore $\frac{B}{2A} \leq +1$. Two possibilities are now contemplated.

(1) If $\frac{B}{2A} < -1, \xi_2 \leq \frac{B}{2A} < -1 \Rightarrow |\xi_2| > 1$: the approximation is unstable. However, this situation cannot be satisfied: $\frac{B}{2A}$ cannot be less than -1.

(2) If $-1 \leq \frac{B}{2A} \leq +1$, the only useful inequality, $-1 \leq \frac{B}{2A}$, is always satisfied.

(2.1) If $B^2 + 4A^2 - 8A \leq 0$, and hence if $\tau^2 \leq \pi^2h^2 - 4(\nu b)^2\pi^2/c_0^2\lambda^2$, then the roots of the equation can be written

$$\xi_1 = \frac{B}{2A} + i\left(\frac{8A - 4A^2}{4A^2} - \frac{B^2}{4A^2}\right)^{1/2}$$
$$\xi_2 = \frac{B}{2A} - i\left(\frac{8A - 4A^2}{4A^2} - \frac{B^2}{4A^2}\right)^{1/2} \tag{25}$$

and thus $|\xi_1| = |\xi_2| = (\frac{8A-4A^2}{4A^2})^{1/2}$. $A \geq 1$ implies $|\xi_1| = |\xi_2| \leq 1$. It can be seen that A is always greater than or equal to 1 and so in this case $|\xi_1| = |\xi_2| \leq 1$ is always satisfied.

(2.2) If $B^2 + 4A^2 - 8A > 0$. This inequality cannot be satisfied.

Finally, the inequality

$$\tau^2 \leq \pi^2h^2 - \frac{4(\nu b)^2\pi^2}{c_0^2\lambda^2} \tag{26}$$

is the stability condition. Thus the finite-difference approximation is conditionally stable. Figure 2 shows the domains of stability and instability performed by the von Neumann stability analysis with $f = 20$ kHz, $\alpha = 1.81$ m^{-1}, and $c_0 = 340$ m/s. A useful relation between h and τ that satisfies the stability condition is employed in the simulations:

$$\tau = \frac{-\nu b\pi}{c_0\lambda} + \pi\sqrt{\frac{(\nu b)^2}{c_0^2\lambda^2} + h^2}. \tag{27}$$

It is also represented in Fig. 2.

The numerical scheme obtained for u_2 can be written

$$\begin{aligned} -\mathrm{A}u_{m-1,n} + (2\mathrm{A}+1)u_{m,n} - \mathrm{A}u_{m+1,n} = {} & -\mathrm{A}u_{m-1,n-2} + (2\mathrm{A}-1)u_{m,n-2} - \mathrm{A}u_{m+1,n-2} \\ & + \mathrm{B}u_{m-1,n-1} + 2(1-\mathrm{B})u_{m,n-1} \\ & + \mathrm{B}u_{m+1,n-1} + K_{u_{1_{n-1}}} \end{aligned} \tag{28}$$

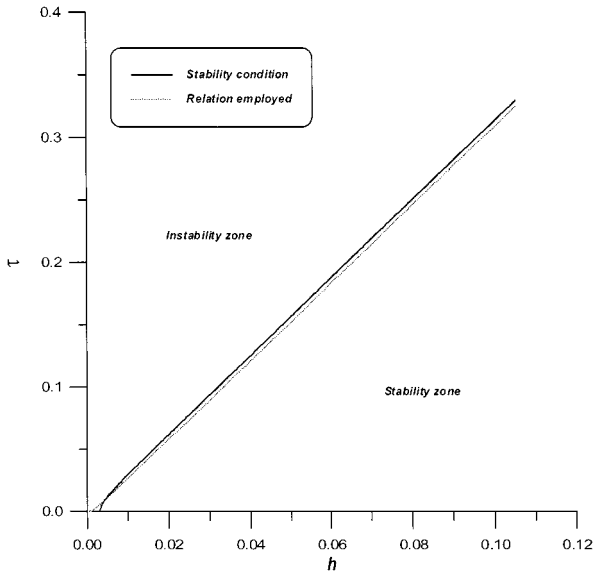

FIG. 2. Stability and instability zones produced by the von Neumann analysis. For the representation, $f = 20$ kHz, $\alpha = 1.81$ m^{-1} and $c_0 = 340$ m/s. Comparison of the von Neumann criterion with the relation between h and τ employed during the simulations.

with $\mathrm{A} = \nu b\tau/\pi c_0 \lambda h^2 = (\nu b/\pi c_0 \lambda)(\tau/h^2) = aX$, $\mathrm{B} = \tau^2/\pi^2 h^2 = (1/\pi^2)(\tau^2/h^2) = bY$; $a > 0, b > 0, X > 0, Y > 0$. $K_{u_{l_{n-1}}} = C[(u_{l_{m+1,n-1}} - u_{l_{m,n-1}})^2 - (u_{l_{m,n-1}} - u_{l_{m-1,n-1}})^2]$, where $C = c_0^2(\gamma + 1)\tau^2/2\omega^2 L^3 h^3$, issues from the calculations of u_l and is considered to be a constant. The constant $K_{u_{l_{n-1}}}$ does not influence the von Neumann analysis. Therefore this analysis yields to the same criterion as for u_l.

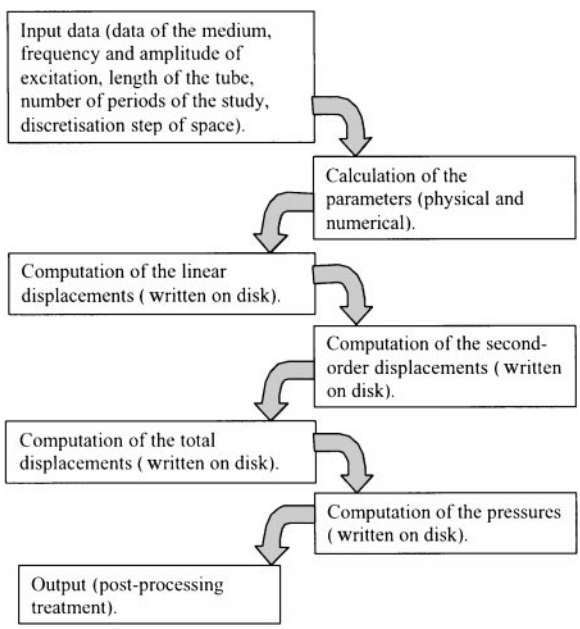

FIG. 3. Procedure of the computational code.

The analysis of stability has shown the usefulness of the relation (27) between τ and h; when this relation is employed, the finite-difference approximation is stable. As shown before, the finite-difference equations are both consistent with the partial differential equations. So when the relation (27) between τ and h is employed, it follows that the finite-difference approximation is convergent [21]. An example of the convergence of the scheme is shown in Section 4.B.

A value of τ less than the value used by the relation (27) could also ensure the stability (see Fig. 2). Nevertheless the relation (27) automatically fixes the τ values very close to the stability bound.

Figure 3 shows the schematic representation of the algorithm. The space reserved for the writing on disk is $(217 * \mathrm{NPT} * \mathrm{NPS})/(1024^2)$ Mbytes. This storage includes two files (for displacement and pressure) written by columns, which make the posttreatment easier.

4. RESULTS

In this section, the algorithm presented above is illustrated. All the computations were run on a processor Pentium II MMX of 300 MHz and 64 MB Ram. CPUt means the running time of a simulation using this processor. This time includes an analytical calculation of the linear solution at grid-points and an evaluation of its maximum value in order to get a reference for fast comparisons with the nonlinear values.

4.A. *Validation*

In this section, results from the numerical algorithm are compared with results produced by an analytical model. This analytical model is also a perturbation model and Eqs. (8) and (9) are solved in the frequency domain; i.e., an equation is written and solved for every frequency studied. The approximation $\alpha \ll k$ is also assumed (where $\alpha = \omega^2 \nu b/2c_0^3$ and $k = \omega/c$), and then all terms of order α^2 or less are neglected.

With this approximation the following solution is obtained for Eq. (8) and the boundary conditions (11a),

$$u_1 = u_0 \cos\, \omega t \frac{\sin k(L-x)}{\sin\, kL}, \tag{29}$$

where $k = k_0 - i\alpha$, $k_0 = \frac{\omega}{c_0}$. By substituting solution (29) into Eq. (9) we obtain the second order correction

$$\begin{aligned} u_2 = {} & \cos(2\omega t)[C_1 \cos((2k_0 - i4\alpha_0)(L-x)) + C_2 \sin((2k_0 - i4\alpha_0)(L-x))] \\ & + (D_1 x + D_2) + C_3 \cos(2\omega t)(L-x)\cos k_n(L-x) + D_3 \sin 2k(L-x) \end{aligned} \tag{30}$$

with $k_n = 2k_0 - i\alpha_n$, where C_1, C_2, C_3, D_1, D_2, D_3, and α_n are indefinite constants. C_1, C_2, D_1, and D_2 are obtained from the boundary conditions, and C_3, D_3, and α_n by substituting Eq. (30) into the wave equation (9). For the perturbation u_2 we consider a rigid-ended tube because the piston is harmonically vibrating (boundary conditions (11b)),

$$\begin{aligned} C_1 &= 0 & D_1 &= D_3 \sin 2kL/L \\ C_2 &\cong -j\frac{C_3}{4\alpha_0} & D_2 &= -D_3 \sin 2kL, \end{aligned} \tag{31}$$

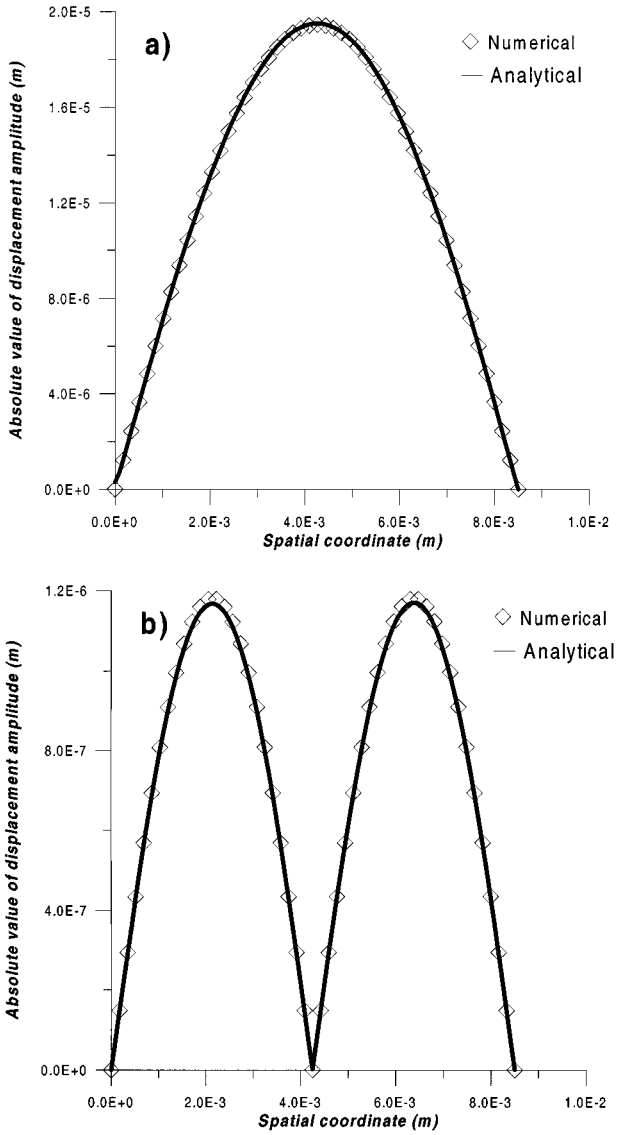

FIG. 4. Comparison between numerical and analytical results for a resonant air-filled tube excited at 20 kHz; $u_0 = 3 \times 10^{-7}$ m; $\alpha = 1.81$ m^{-1}; $L = \lambda/2$. (a) First-order component. (b) Second-order perturbation.

where the assumption of small attenuation has been used. By substituting solution (30) into Eq. (9), using (31) and again neglecting all the terms on the order of α_0^2, α_n^2, and $\alpha_0\alpha_n$ we obtain $C_3 = \frac{(\gamma+1)}{16k_0} \frac{k^3 u_0^2}{\sin^2[kL]}$, $\alpha_n = 2\alpha_0$, and $D_3 = \frac{C_3}{k}$. Even if the treatment of the attenuation is more approximate, important differences are not expected for small attenuation values and tube lengths which are not too large.

Both methods are applied to an air-filled rigid-walled tube ($c_0 = 340$ m/s; $\rho_0 = 1.29$ kg/m^3). The excitation frequency of the piston is 20 kHz and its maximum displacement $u_0 = 3 \times 10^{-7}$ m. We consider $\gamma = 1.6$. As explained above, only bulk attenuation is considered (a ω^2 attenuation dependence), without any limitation on its parameter value α. This fact allows this value to increase in order to take indirectly into account losses due to

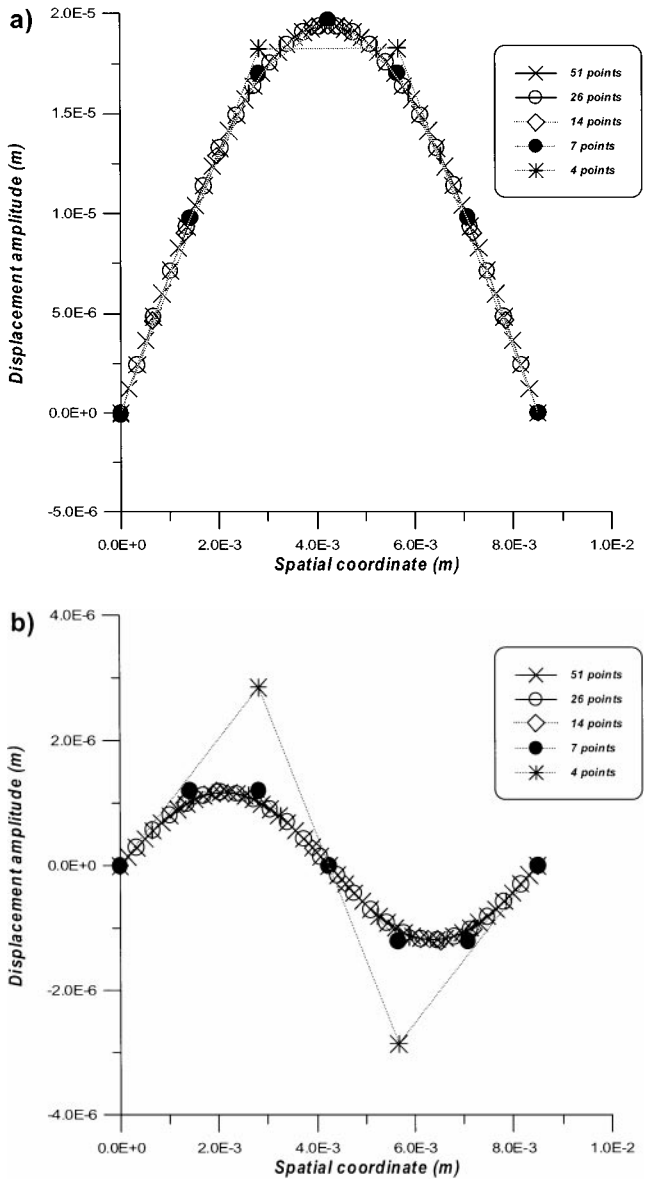

FIG. 5. Convergence study of the scheme at 20 kHz; $u_0 = 3 \times 10^{-7}$ m; $\alpha = 1.81$ m^{-1}; $L = \lambda/2$. (a) Fundamental frequency. (b) Second-order perturbation.

the walls of the tube that are not considered explicitly. The model is effectively applied to narrow tubes in which a large quantity of energy is lost in the walls. So we have to increase the attenuation value to produce a more realistic simulation, which is why $\alpha = 1.81$ m^{-1}, a high value for a free-field problem. The length of the resonant tube is $L = \lambda/2 = 0.0085$ m. For the numerical simulation, the spatial step h is 0.02, and 200 periods (0.01 s) are analysed; in this way, NPS $= 51$ and NPT $= 21620$. CPUt $=$ 2:08:00. The storage used on disk is 228.18 Mbytes. Figure 4 shows the amplitude displacement obtained with both methods. Displacement distributions are compared in Fig. 4a for the first-order approximation and in Fig. 4b for the corresponding second-order perturbation. Excellent agreement between the

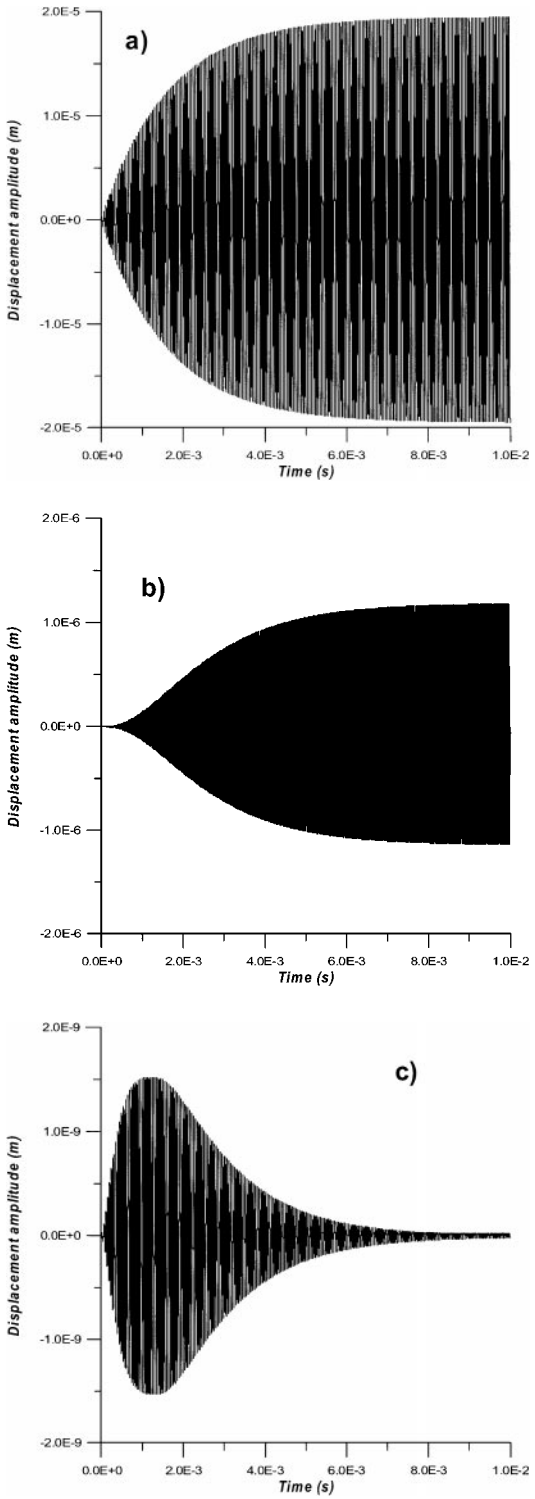

FIG. 6. Temporal evolution of the acoustic wave in the resonant tube from the rest state at 20 kHz; $u_0 = 3 \times 10^{-7}$ m; $\alpha = 1.81$ m^{-1}; $L = \lambda/2$. (a) Fundamental component of the displacement at $\lambda/4$. (b) Second-order component at $\lambda/8$. (c) Second-order component at $\lambda/4$.

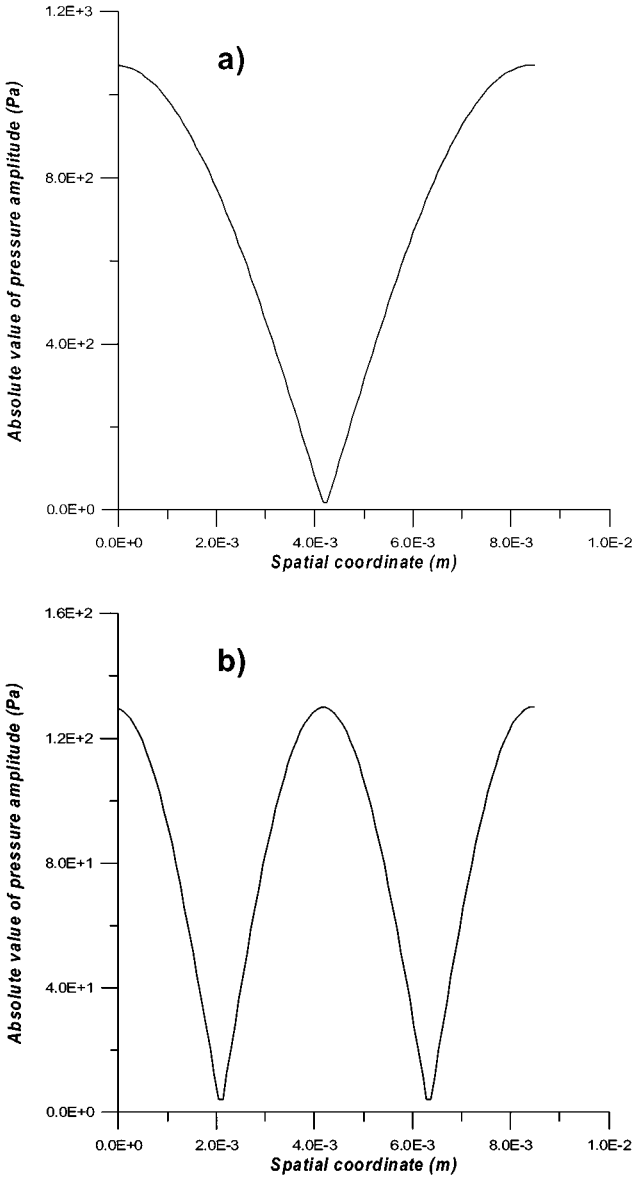

FIG. 7. Distribution of the pressure amplitude at 20 kHz; $u_0 = 3 \times 10^{-7}$ m; $\alpha = 1.81$ m^{-1}; $L = \lambda/2$. (a) Fundamental component. (b) Second-order component.

analytical and numerical methods is observed, which means convergence of the numerical scheme has been obtained and the results we get are coherent with the analytical ones.

4.B. *Convergence Study*

A convergence study was performed analysing the example presented above. We compare the results of using 51 spatial points versus other numbers of points to solve the same problem. A series of calculations was performed with various spatial-grid sizes: 4, 7, 14, 26, and 51 spatial points. Results are shown in Fig. 5. Figure 5a shows the fundamental

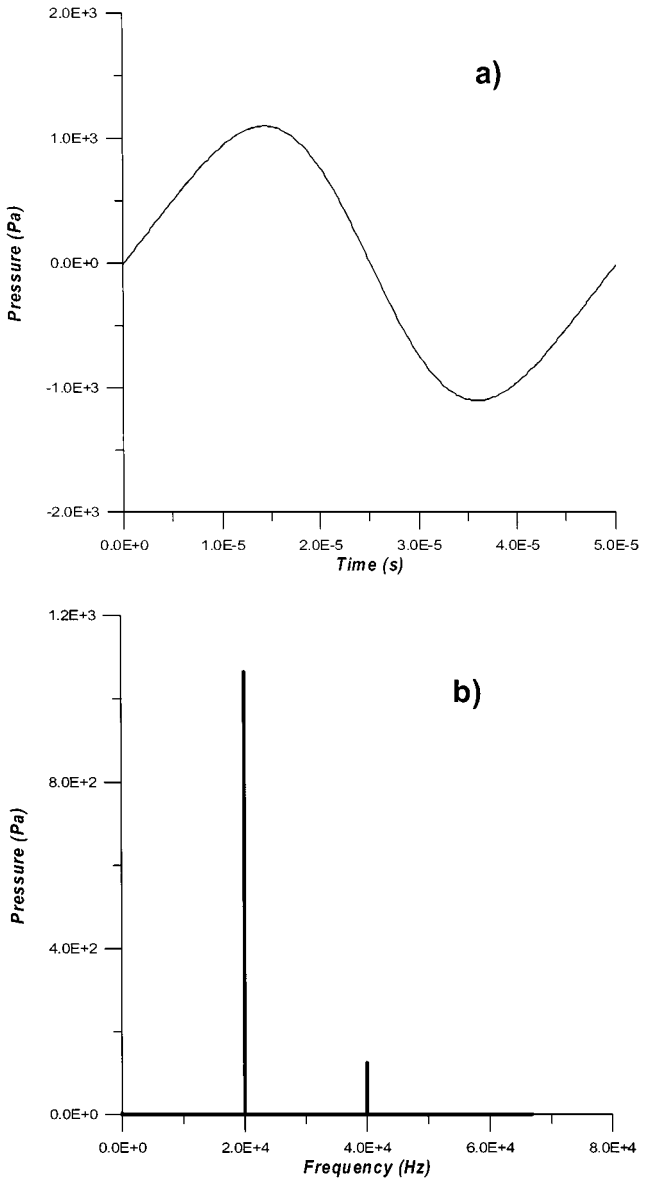

FIG. 8. Wave form (a) and harmonic components (b) of the pressure at the reflector at 20 kHz. $u_0 = 3 \times 10^{-7}$ m. $\alpha = 1.81$ m^{-1}. $L = \alpha/2$.

frequency component and Fig. 5b shows the second-order perturbation. Rapid evolution to convergence can be seen when the number of spatial points grows (see Section 3.B.2.).

4.C. *Examples*

In this section, various results show that the numerical methods presented in Section 3 are well founded. In the first part, the considered resonant rigid-walled tubes have a length of $\lambda/2$, λ being the wavelength corresponding to the excitation frequency; in the second part, $\lambda/2$-, λ-, and $3\lambda/2$–length resonant rigid-walled tubes are studied. All the results presented

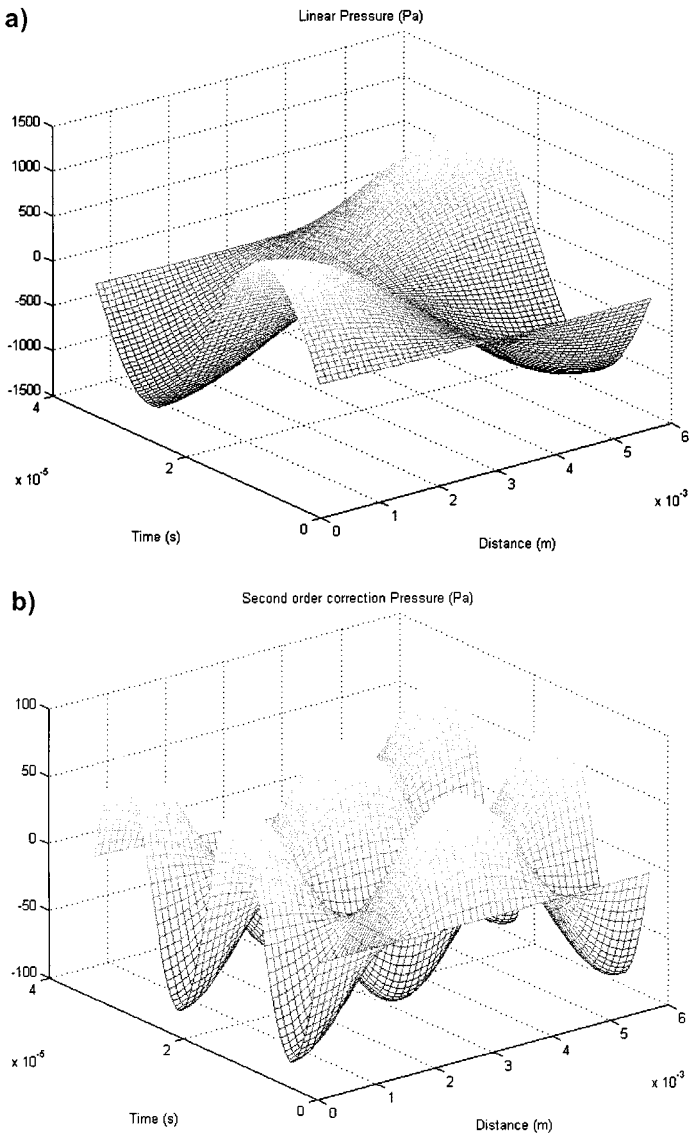

FIG. 9. Amplitude value of the standing pressure at 30 kHz; $u_0 = 3 \times 10^{-7}$ m; $\alpha = 4.07$ m^{-1}; $L = \lambda/2$. (a) Linear pressure. (b) Second-order pressure.

were obtained from simulations performed with a number of spatial points suitable to lead to convergence of the numerical scheme. By modelling the transient stage from starting absolute rest of the fluid, we are able to simulate the whole real problem. Nevertheless, more time grid-points are needed and therefore more CPUt and computer storage capacity.

4.C.1. The same example used to compare the numerical and analytical models (Section 4.A) is considered. Figure 6 shows the temporal evolution of both first (6a) and second-order (6b and 6c) components of the displacement, from the rest state to the stationary wave. Figures 6a and 6b correspond to points at which the component is maximal: at $\lambda/4$ for the linear component and at $\lambda/8$ for the second-order one. Figure 6c shows a

point at which the second-order component is minimal: at $\lambda/4$. At the point of maximal amplitude, the second-order component increases more slowly from the rest state than the fundamental one. Figure 7 shows pressure distributions corresponding to each approximation. The second-order component presents a maximum at the node of the fundamental, while its nodal points correspond to zones where the fundamental does not vanish. This fact means that the nonlinear behaviour of the fluid generates the disappearance of the pressure node in the resonant tube. In the case of a progressive plane wave, it is well known that the distortion of the wave increases with the distance from the source. In the case of a standing wave, the end of the tube closer to the source corresponds to one of the maximal values of the second harmonic. Figure 8a shows the wave shape of the pressure at the reflector ($x = L$). Figure 8b represents the corresponding fast Fourier transform (FFT). We can see that the nonlinear distortion of the wave is due to the double-frequency component.

We now consider an air-filled tube ($c_0 = 340$ m/s, $\gamma = 1.6$, $\rho_0 = 1.29$ kg/m^3) excited at 30 kHz with an amplitude of 3×10^{-7} m; $\alpha = 4.07\ \mathrm{m}^{-1}$. The spatial step is $h = 0.02$. Thus NPS = 51 and NPT = 16856. CPUt is about 1:40:00 for a study of 150 periods. Figure 9 represents the tri-dimensional (distance, time, pressure amplitude) diagram of the pressure throughout a standing period. The second-order correction pressure induces the distortion of the total pressure and the disappearance of the node at the centre of the tube.

Figure 10 shows the evolution of the maximal absolute value of the second-order and total pressure reached during a standing period versus the excitation displacement amplitude. The excitation frequency is 100 kHz, and the medium is air ($c_0 = 340\,\mathrm{m/s}$, $\gamma = 1.6$, $\rho_0 = 1.29$ kg/m^3). In this calculation, a very high attenuation ($\alpha = 45.25\ \mathrm{m}^{-1}$) has been used. Results show the increase of the wave distortion (showing the importance of the second-order component) as u_0 grows. In fact, the second-order component increases according to a quadratic law, while the fundamental component increases according to a

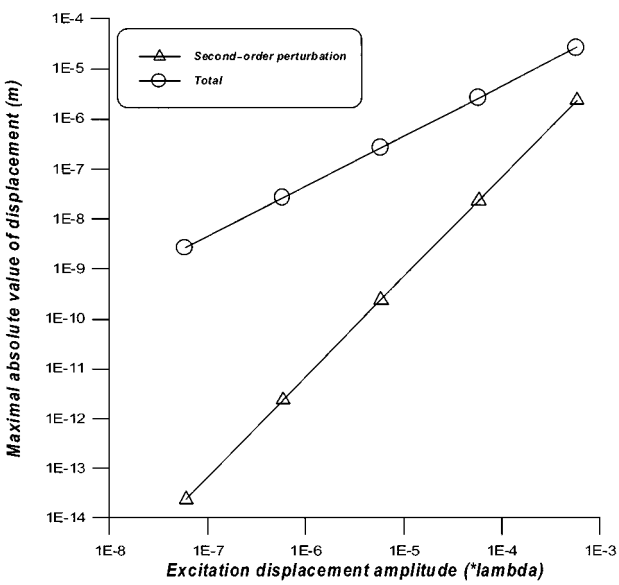

FIG. 10. Absolute value of the second-order perturbation and total displacement at 100 kHz; $\alpha = 45.25\ \mathrm{m}^{-1}$; $L = \lambda/2$. Evolution of its maximum versus u_0.

linear law, with regard to the excitation amplitude. Saturation does not occur in the range of amplitudes for which a second-order perturbation model is valid.

4.C.2. Other air-filled tubes are now considered ($c_0 = 340$ m/s, $\gamma = 1.6$, and $\rho_0 = 1.29$ kg/m^3). The excitation frequency is 20 kHz and $\alpha = 1.81$ m^{-1}. Figure 11 shows the space representation of the standing pressure for three tubelengths: $\lambda/2$ (1), $2 \cdot \lambda/2$ (2), and $3 \cdot \lambda/2$ (3). For all the cases, the displacement of the piston is the same, $u_0 = 0.3\ \mu$m, and the representation is shown at the time of maximal pressure during a standing period. Figure 11a shows to the fundamental frequency and Fig. 11b shows the second-order components. Results clearly show the change in the distribution of the pressure along the tube and the

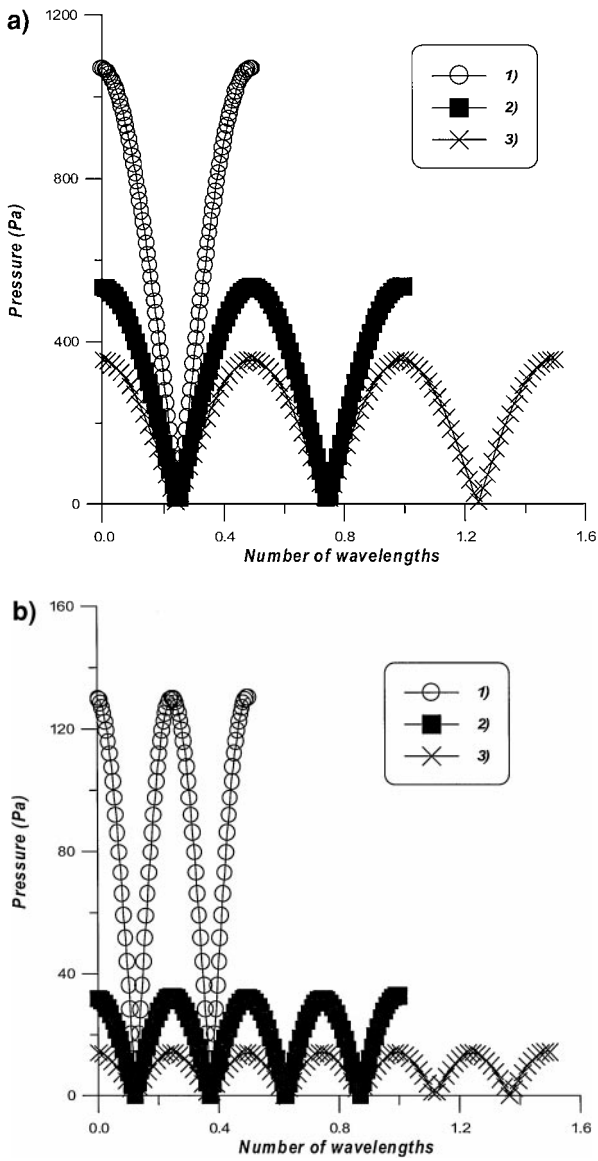

FIG. 11. Pressure distribution for three tubelengths at 20 kHz; $u_0 = 0.3\ \mu$m; $\alpha = 1.81$ m^{-1}. (1) $L = \lambda/2$. (2) $L = 2 \cdot \lambda/2$. (3) $L = 3 \cdot \lambda/2$. (a) Fundamental frequencies. (b) Second-order components.

decrease of the nonlinearity as the length increases (the importance of the second-order component in relation to the fundamental decreases).

5. CONCLUSION

A numerical algorithm based on the finite-difference method has been presented. It allows the modelling of finite but moderate amplitude standing acoustic waves in the time domain. The numerical method has been validated by comparison with an analytical model. Various kinds of results show the efficiency and limits of the simulating code. This procedure opens a new framework of development for the modelling and design of high-power ultrasonic processing systems. More sophisticated versions of the code, which include higher order nonlinearity (weak shock approximation [25]), geometrical variations of the resonator, and more complicated dispersion relationships, are currently under development.

REFERENCES

1. E. Fubini-Ghiron, Anomalies in the propagation of an acoustic wave of larger amplitude, *Alta Freq.* **4**, 532 (1935). English version by R. T. Beyer in [6].
2. D. T. Blackstock, On plane, spherical and cylindrical sound waves of finite amplitude in lossless fluids, *J. Acoust. Soc. Am.* **36**, 217 (1964).
3. W. Chester, Resonant oscillations in closed tubes, *J. Fluid Mech.* **18**, 44 (1964).
4. A. B. Coppens and J. V. Sanders, Finite-amplitude standing waves in rigid-walled tubes, *J. Acoust. Soc. Am.* **43**, 516 (1968).
5. R. T. Beyer, Nonlinear acoustics, in *Physical Acoustics*, edited by W. P. Mason (Academic Press, New York, 1965), Vol. II, Part. B, p. 231.
6. R. T. Beyer, *Nonlinear acoustics in fluids*, Benchmark Papers in Acoustics Series (Van Nostrand-Reinhold, New York, 1984).
7. L. Bjorno, Nonlinear acoustics, in *Acoustics and Vibration Progress*, edited by R. W. B. Stephen and H. G. Leventhall (Chapman & Hall, London, 1976), Vol. 2, p. 101.
8. O. V. Rudenko and S. I. Soluyan, *Theoretical Foundations of Nonlinear Acoustics* (Consultants Bureau, New York, 1977).
9. M. F. Hamilton and D. T. Blackstock, Eds., *Nonlinear Acoustics* (Academic Press, San Diego, 1998).
10. B. Dubus, A. Lavie, D. Décultot, and G. Maze, Coupled finite element method/boundary element method for the analysis of the acoustic scattering from elastic targets, in *ASME 15th Biennial Conf. on Mechanical Vibration and Noise: Acoustics of Submerged Structures and Transduction Systems, Vienna*, 1995, Vol. 3, Part B, p. 25.
11. C. Vanhille and A. Lavie, An efficient tool for multi-frequency analysis in acoustic scattering or radiation by boundary element method, *Acustica united with Acta Acustica* **84**, 884 (1998).
12. A. Lavie and B. Dubus, *Méthodes Numériques en Diffusion Acoustique*, 3ième École d'Hiver sur la Diffusion Acoustique, Cauterets (1996).
13. R. O. Cleveland, M. F. Hamilton, and D. T. Blackstock, Time-domain modeling of finite-amplitude sound in relaxing fluids, *J. Acoust. Soc. Am.* **99**, 3312 (1996).
14. B. E. McDonald and W. A. Kuperman, Time-domain formulation for pulse propagation including nonlinear behavior at a caustic, *J. Acoust. Soc. Am.* **81**, 1406 (1987).
15. Yang-Sub Lee and M. F. Hamilton, Time-domain modeling of pulsed finite-amplitude sound beams, *J. Acoust. Soc. Am.* **97**, 906 (1995).
16. C. Campos-Pozuelo, B. Dubus, and J. A. Gallego-Juárez, Finite-element analysis of the nonlinear propagation of high-intensity acoustic waves, *J. Acoust. Soc. Am.* **106**, 91 (1999).
17. Y. A. Ilinskii, *et al.*, Nonlinear standing waves in an acoustical resonator, *J. Acoust. Soc. Am.* **104**, 2664 (1998).

18. C. Vanhille and C. Campos-Pozuelo, Ondas acústicas estacionarias: Aproximación de segundo orden, in *Actas del XVI Congreso de Ecuaciones Diferenciales y Aplicaciones, VI Congreso de Matemática Aplicada, Las Palmas de Gran Canaria, Spain, 1999*, edited by R. Montenegro, G. Montero, and G. Winter, Vol. II, p. 1323.
19. P. M. Morse and K. U. Ingard, *Theoretical Acoustics* (McGraw–Hill, New York, 1968).
20. D. A. Sullivan, Historical review of real-fluid isentropic flow models, *J. Fluids Eng.* **103**, 258 (1981).
21. G. D. Smith, *Numerical Solution of Partial Differential Equations, Finite Difference Methods*, 3rd ed. (Clarendon, Oxford, 1985).
22. W. E. Milne, *Numerical Solution of Differential Equations* (Dover, New York, 1970).
23. D. M. Young and R. T. Gregory, *A Survey of Numerical Mathematics*, Vol. II (Dover, New York, 1988).
24. L. Lapidus and G. F. Pinder, *Numerical Solution of Partial Differential Equations in Science and Engineering* (Wiley–Interscience, New York, 1999).
25. C. Vanhille and C. Campos-Pozuelo, A time-domain numerical algorithm for the analysis of nonlinear standing acoustic waves, in *Nonlinear Acoustics at the Turn of the Millenium*, edited by W. Lauterborn and T. Kurz (American Institute of Physics, Melville, New York, 2000), p. 177.